

Domain-Skewed Federated Learning with Feature Decoupling and Calibration

Huan Wang^{1,2} Jun Shen^{1*} Jun Yan¹ Guansong Pang^{2*}

¹School of Computing and Information Technology, University of Wollongong, Australia

²School of Computing and Information Systems, Singapore Management University, Singapore

hw226@uowmail.edu.au, jshen@uow.edu.au, jyan@uow.edu.au, gspang@smu.edu.sg

Abstract

Federated learning (FL) allows distributed clients to collaboratively train a global model in a privacy-preserving manner. However, one major challenge is domain skew, where clients' data originating from diverse domains may hinder the aggregated global model from learning a consistent representation space, resulting in poor generalizable ability in multiple domains. In this paper, we argue that the domain skew is reflected in the domain-specific biased features of each client, causing the local model's representations to collapse into a narrow low-dimensional subspace. We then propose **Federated Feature Decoupling and Calibration (F²DC)**, which liberates valuable class-relevant information by calibrating the domain-specific biased features, enabling more consistent representations across domains. A novel component, **Domain Feature Decoupler (DFD)**, is first introduced in F²DC to determine the robustness of each feature unit, thereby separating the local features into domain-robust features and domain-related features. A **Domain Feature Corrector (DFC)** is further proposed to calibrate these domain-related features by explicitly linking discriminative signals, capturing additional class-relevant clues that complement the domain-robust features. Finally, a domain-aware aggregation of the local models is performed to promote consensus among clients. Empirical results on three popular multi-domain datasets demonstrate the effectiveness of the proposed F²DC and the contributions of its two modules. Code is available at <https://github.com/mala-lab/F2DC>.

1. Introduction

Federated Learning (FL) [22, 31] is emerging as a privacy-preserving technique for collaboratively training a shared global model on multiple clients without leaking privacy. The FL approaches are embodied by key cornerstone algorithms such as FedAvg [31], where each client executes

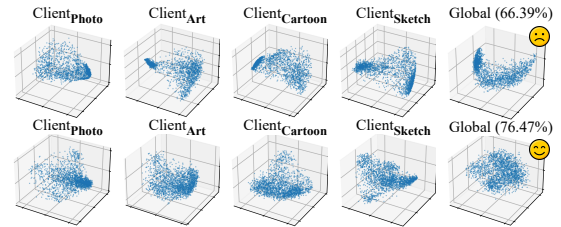


Figure 1. Visualization of the singular values of the feature covariance matrix on the PACS [19] dataset from Vanilla FL [31] (**Top**) and our method (**Bottom**). Under domain-skewed FL, the Vanilla method suffers from severe dimensional collapse, *i.e.*, representations are largely biased and reside in a domain-specific lower-dimensional subspace. Our method effectively mitigates this collapse, as reflected in more uniformly distributed singular values and significantly fewer values tending to zero.

stochastic gradient descent iterations to minimize the local empirical objective, and all participating clients' local models are then sent to the server to perform global aggregation of parameters. An inherent challenge in the FL paradigm is the potential discrepancies of local data distributions among clients, referred to as *data heterogeneity* [16, 21, 22, 58]. In particular, clients have drastically different data preferences collected from distinct sources, resulting in non-independent and identically distributed (non-iid) data distribution [21, 58]. Such data heterogeneity has caused the global model to perform poorly [23, 25].

To alleviate the data heterogeneity problem, subsequent studies focus on stabilizing local training [17, 23, 43] or regulating global aggregation [42, 47, 51] to reduce the variance in the FL optimization. Notably, these methods primarily consider a *label skew* issue, *i.e.*, data class distributions are different among clients while all data originate from the same domain. However, for many real-world scenarios (*e.g.*, driving data collected from different vehicles under diverse weather conditions), the data heterogeneity is predominated by *domain skew*, where the local data among different clients are drawn from varying domains but have a similar class distribution. This often leads to severe *dimen-*

*Corresponding Authors: Jun Shen, Guansong Pang

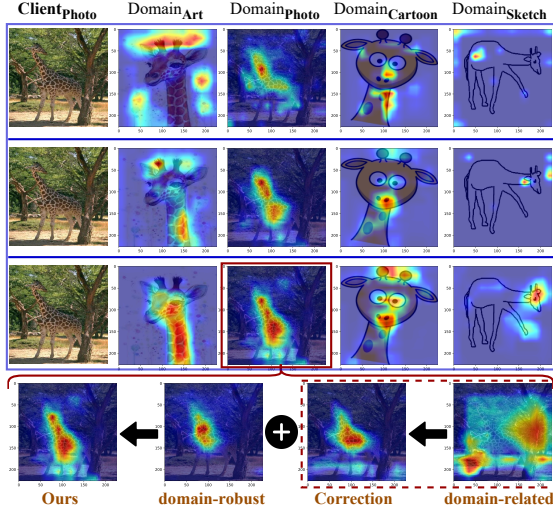


Figure 2. Grad-CAM [35] visualization of the features obtained by three methods—Vanilla method [31] (Top), domain-skewed method FDSE [48] (Middle), and F^2DC (Bottom)—for samples from different domains on a randomly selected $Client_{photo}$ belonging to the photo domain. For our method F^2DC , we further provide a qualitative example about how its two modules work: local features are first decoupled via DFD into domain-robust features and domain-related features (which entangle valuable class-relevant information with domain biases). Then, the domain-related features (which entangle valuable class-relevant information with domain biases) are calibrated via DFC, resulting in the Correction features. By incorporating the domain-robust and the corrected features, F^2DC captures more holistic class-relevant clues, enabling the local model to yield more consistent decisions for samples with the same semantics across different domains.

sional collapse in local model training due to their exclusive fitting to the features of individual domains in each client, and consequently, the representations in each client mainly reside in a narrow low-dimensional subspace, ignoring relevant features in the other subspaces. This issue manifests as small (near-zero) singular values of the feature covariance matrix in each client, as illustrated in Fig. 1-Top. Aggregating from such domain-biased local models can result in a great difficulty to obtain consensus updates in the global model, rendering it ineffective in generalizing to data from different domains, as exemplified by the large discrepancy in the attended features across the domains in Fig. 2-Top. This motivates the question: *Can we promote local training away from client-specific domain preferences under the domain-skewed FL scenario?*

To address this challenge, recent advanced FL methods [7, 48] aim to eliminate and deactivate domain-specific biases from the local parameters to improve performance and facilitate consensus updates. However, these ‘elimination-based’ methods risk discarding additional class-relevant information that is entangled with these domain-specific fea-

tures, *e.g.*, FDSE [48] misses the antlers and head of the giraffe in the cartoon and sketch domains in Fig. 2-Middle. This motivates our **core question**: *Can we correct domain-specific biases to capture additional class-relevant features, thus promoting a more domain-generalizable global model?*

To overcome this domain skew issue, we propose F^2DC , namely **Federated Feature Decoupling and Calibration**, aiming to correct domain-specific biased features to improve the generalizable ability of local training. F^2DC consists of two novel modules, including Domain Feature Decoupler (DFD) and Domain Feature Corrector (DFC). DFD is optimized to decouple the local features into *domain-robust features* that focus on discriminative cross-domain class-relevant information, and *domain-related features* that are responsible for the client-specific domain context. This prevents F^2DC from overfitting the domain-biased features, as shown in Fig. 1-Bottom. Further, the domain-related features inherently entangle domain biases (*e.g.*, the stroke style of a sketch domain) with class-relevant information (*e.g.*, the ‘object outline’ formed by the sketch). To capture these additional class-relevant clues that can complement the domain-robust features, DFC is devised to calibrate these domain-related features by explicitly linking correct semantic signals. Finally, we perform domain-aware aggregation of the local models to incorporate the domain discrepancy into the global model, thereby further promoting consensus among clients. As shown in Fig. 2-Bottom, F^2DC can more consistently obtain discriminative features across domains compared to [31, 48]; to zoom in the photo domain example, DFD in F^2DC accurately decouples the domain-robust features (the upper giraffe body) from the domain-related features, and it further captures the additional class-relevant clues (*e.g.*, correction features recapture the giraffe’s waist) from the noisy domain-related features via DFC. The main contributions are listed below:

- Rather than eliminating domain-specific biases as recent domain-skewed FL methods do, we argue that these biases are inherently entangled with valuable class-relevant information, once properly calibrated, can be leveraged to produce more consistent decisions across domains.
- We propose F^2DC , a novel solution for domain-skewed FL. It improves cross-domain performance by decoupling and correcting the local features through its two novel modules DFD and DFC, while performing domain-aware aggregation to promote more consensus among clients.
- Extensive experiments conducted on three multi-domain datasets demonstrate that F^2DC consistently outperforms state-of-the-art methods. Comprehensive ablation studies also confirm the contributions of its two modules.

2. Related Work

Heterogeneous Federated Learning. Federated learning has been an emerging topic that collaboratively trains a

shared global model without sharing private data [21, 23, 31]. However, due to the data heterogeneity, this paradigm suffers from unstable, slow convergence [9, 14, 21, 25, 58]. To tackle this, previous studies either regularize local training at the client-side [12, 13, 44, 45, 49] or adjust global aggregation at the server-side [11, 42, 47, 51, 52]. However, most of these methods neglect the domain skew, leading to compromised performance on multiple domains [5, 13].

Domain-Skewed Federated Learning. Domain-skewed data readily weakens the generalization of the global model, which has motivated the development of domain-skewed FL [5, 6, 13, 37, 48, 54, 57]. To mitigate the domain skew, there are mainly two directions: enhancing the uniformity between clients [5, 13, 15, 57] and personalizing the global model [27, 28, 38]. FedSA [57] builds anchor-based regularization to ensure consistent boundaries across domains. FedHEAL [5] leverages selective parameter local updating and a fair aggregation objective to facilitate fairness and performance. FDSE [48] decouples each model layer into a domain-agnostic extractor and a domain-specific eraser, achieving global consensus and local personalization. However, these methods aim to discard or deactivate the domain-biased parameter updates of the local training, ignoring useful clues that may exist in the domain context. In contrast, we claim that, with proper correction, the domain-related features of each client can recapture additional useful guidance to promote cross-domain generalizability.

Disentangled Representation Learning. Disentangled representation learning (DRL) aims to learn a mechanism to identify and disentangle latent factors hidden in the data at the feature-level [8, 46, 56]. Previous works are focused on separating general and individual features for downstream tasks, such as gait recognition [26, 56], recommendation [30], graph analysis [32, 55], etc. There are also some works that incorporate disentangled learning into federated learning [1, 2, 4, 39, 50] to assist local training in FL to achieve higher performance. However, these methods focus on single-domain performance. Under a domain skew FL scenario, it is essential to consider generalization across different domains. Our work illustrates how to leverage the disentangled learning (*i.e.*, local feature decoupling and correction) to tackle the domain skew challenge in FL.

3. Problem Statement

Following [5, 13], we focus on the standard domain-skewed FL scenario for K participating clients associated with data partitions $\{\mathcal{D}_1, \dots, \mathcal{D}_k, \dots, \mathcal{D}_K\}$, where each client’s data samples $\mathcal{D}_k = \{x_i, y_i\}_{i=1}^{n_k}, y_i \in \{1, \dots, \mathbb{C}\}$ only belonging to a single domain, n_k denotes the local data scale for client k , and \mathbb{C} denotes the number of categories. Let n_k^c be

the number of samples with class c on client k , we further define $\mathcal{D}_k^c = \{(x_i, y_i) \in \mathcal{D}_k | y_i = c\}$ as the set of samples with class c on client k , where $n_k^c = |\mathcal{D}_k^c|$. The number of samples in class c of all clients is $n^c = \sum_{k=1}^K n_k^c$. Formally, the optimization objective of the domain-skewed FL is:

$$w^* = \arg \min_w \mathcal{L}(w) = \sum_{k=1}^K \frac{n_k}{N} \mathcal{L}_k(w; \mathcal{D}_k), \quad (1)$$

where w is the parameters of the global model, \mathcal{L}_k denotes the empirical objective on the client k , and $N = \sum_{k=1}^K n_k$ denotes the total number of samples among all clients. The optimization objective in Eq. (1) is to learn a generalizable global model w^* to present favorable performance on multiple domains during the FL process. In the FL training setup, for each client k , we consider the local model with parameters $w_k = \{\Phi_k, \theta_k\}$. It has two modules: a feature extractor $r(\Phi_k; \cdot) : x \rightarrow \mathbb{R}^d$, that encodes each sample x to a d -dim embedding $z = r(\Phi_k; x)$; a classifier $h(\theta_k; \cdot) : \mathbb{R}^d \rightarrow \mathbb{R}^{\mathbb{C}}$, that maps the embedding z into a \mathbb{C} -dim logit $\ell = h(\theta_k; z)$.

Domain Skew. In heterogeneous FL scenario, the feature distributions $\mathbb{P}(x|y)$ differ across clients even when $\mathbb{P}(y)$ is consistent, leading to the domain skew problem [13]:

$$\mathbb{P}_{k_1}(x|y) \neq \mathbb{P}_{k_2}(x|y), \quad \text{s.t.} \quad \mathbb{P}_{k_1}(y) = \mathbb{P}_{k_2}(y). \quad (2)$$

4. Methodology

To promote cross-domain generalization ability in domain-skewed FL, we propose F^2 DC. As illustrated in Fig. 3, F^2 DC consists of two main modules, Domain Feature Decoupler (DFD) and Domain Feature Corrector (DFC). First, DFD determines the robustness of each feature unit, thereby separating the local features into domain-robust features and domain-related features (Sec. 4.1). Then, DFC calibrates the domain-related features, enabling the local model to capture additional useful clues for improving decisions across domains (Sec. 4.2). Finally, we perform global aggregation in a domain-aware manner to encourage consensus among local clients (Sec. 4.3).

4.1. Domain Feature Decoupler (DFD)

Our key insight lies in calibrating biased domain-related features during the local training. To this end, our initial step is to isolate these domain-related features from the local features, which capture the client-specific domain context for subsequent calibration. With the above definitions in Sec. 3, for the client k , we further refine the feature extractor $r(\Phi_k; \cdot)$ as backbone layers r_k^B and flatten layers r_k^F : taking ResNet-10 [10] as an example, r_k^B includes 4 backbone layers $L_1 \sim L_4$, r_k^F consists of a pooling layer and a flattening operation. Given an instance $(x_i, y_i) \in \mathcal{D}_k$, we first calculate the feature map $f_i = r_k^B(x_i) \in \mathbb{R}^{C \times H \times W}$ (*e.g.*, for ResNet-10 [10] on PACS [19], $f_i \in \mathbb{R}^{512 \times 16 \times 16}$).

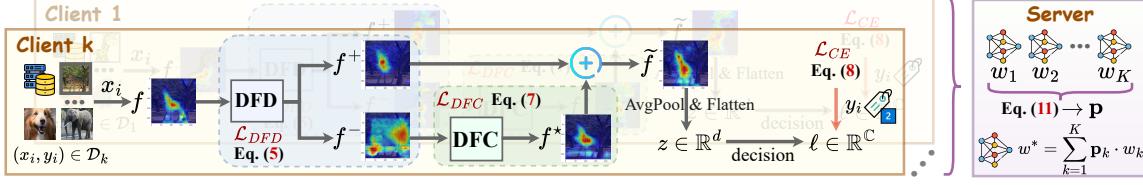


Figure 3. **Overview** of the proposed F^2DC approach. During client-side local training, we initially separate local features into domain-robust features and domain-related features via a Domain Feature Decoupler (DFD) (Sec. 4.1), and then rectify the domain-related features via a Domain Feature Corrector (DFC) (Sec. 4.2). During server-side global aggregation, we perform domain-aware aggregation (Sec. 4.3) of the global model by incorporating each client’s domain discrepancy \mathbf{p}_k to promote more consensus among local clients.

To determine which feature unit of f_i is domain-robust or domain-related, we introduce a Domain Feature Decoupler (DFD) \mathcal{A}_D to construct an attribution map $\mathcal{S}_i = \mathcal{A}_D(f_i) \in \mathbb{R}^{C \times H \times W}$, which quantifies cross-domain robustness score of each feature unit in the f_i . We implement the decoupler \mathcal{A}_D as a two-layer CNN architecture with batch normalization and ReLU activation. To decompose f_i in a complementary manner, we further generate a binary mask matrix $\mathcal{M}_i = \{0, 1\}^{C \times H \times W}$ based on \mathcal{S}_i . The direct strategy is to binarize each element in \mathcal{S}_i into 0 or 1, but such hard discretization would lead to non-differentiability in training [3]. To avoid this problem, we leverage a Gumbel concrete distribution [29] to generate \mathcal{M}_i , defined as:

$$\mathcal{M}_i = \frac{e^{\frac{1}{\sigma}(\log(\epsilon(\mathcal{S}_i)) + \mathbf{g}_a)}}{e^{\frac{1}{\sigma}(\log(\epsilon(\mathcal{S}_i)) + \mathbf{g}_a)} + e^{\frac{1}{\sigma}(\log(1 - \epsilon(\mathcal{S}_i)) + \mathbf{g}_b)}}, \quad (3)$$

where \mathbf{g} is a Gumbel noise $\mathbf{g} = \log(u) - \log(1 - u)$ and $u \sim \mathcal{U}(0, 1)$, σ is used to adjust the smoothness of \mathbf{g}_a and \mathbf{g}_b ($\sigma \rightarrow 0$, \mathcal{M}_i is approximately a hard discretization), ϵ is a Sigmoid function, and e denotes an Exponential function.

On the basis of Eq. (3), a pseudo-binary mask matrix \mathcal{M}_i is generated based on the Gumbel score of \mathcal{S}_i , where the element’s value of \mathcal{M}_i close to 1 indicates a domain-robust feature unit and close to 0 as a domain-related feature unit. We then decouple the local feature map f_i via \mathcal{M}_i as:

$$f_i^+ = \mathcal{M}_i \odot f_i, \quad f_i^- = (1 - \mathcal{M}_i) \odot f_i, \quad (4)$$

where \odot represents an element-wise product operator, the f_i^+ and f_i^- are domain-robust and domain-related features.

On the one hand, we expect to ensure decent separation between f_i^+ and f_i^- to provide class-relevant information and biased domain context. On the other hand, we emphasize maintaining discriminative ability. Consequently, we encourage the learning of \mathcal{A}_D by:

$$\mathcal{L}_{DFD} = \underbrace{\log(\exp(\mathbf{s}(l_i^+, l_i^-)/\tau))}_{\text{Separability}} - \underbrace{(y_i \cdot \log(\delta(\mathbf{m}(l_i^+))) + \hat{y}_i \cdot \log(\delta(\mathbf{m}(l_i^-))))}_{\text{Discriminability}}, \quad (5)$$

$$\text{s.t. } l_i^+ = r_k^F(f_i^+) \in \mathbb{R}^d, \quad l_i^- = r_k^F(f_i^-) \in \mathbb{R}^d,$$

$$\text{s.t. } \mathbf{s}(l_i^+, l_i^-) = (l_i^+ \cdot l_i^-) / (\|l_i^+\|_2 \times \|l_i^-\|_2),$$

where r_k^F consists of a pooling layer and a flattening operation as $\mathbb{R}^{C \times H \times W} \rightarrow \mathbb{R}^d$, \mathbf{s} denotes calculating cosine similarity, \mathbf{m} is a trainable single-layer MLP architecture as $\mathbb{R}^d \rightarrow \mathbb{R}^C$ to predict the logits of f_i^+ and f_i^- , \hat{y}_i represents the wrong label with the highest confidence except the ground truth y_i , τ is used to control the concentration strength of representations [41] to help suitably separate the f_i^+ and f_i^- , and δ represents a Softmax function.

By minimizing Eq. (5), we optimize \mathcal{A}_D to assign higher elements to f_i^+ via \mathcal{M}_i in Eq. (3), which encourages \mathbf{m} to make correct decisions. Meanwhile, \mathcal{A}_D reduces the attention of domain-related features f_i^- to the semantic object, shifting the focus toward the client-specific domain context that may cause wrong decisions. Notably, this domain context can contain some inherently entangled class-relevant information and noisy domain biases, on which \mathcal{A}_D cannot perfectly isolate all discriminative signals into f_i^+ , *i.e.*, \mathcal{A}_D inevitably relegates those ‘mixed’ features into f_i^- . Therefore, the resulting f_i^- is often a complex mixture of domain artifacts and valuable class-relevant clues. This point is empirically verified in two directions: 1) enforcing an overly aggressive separation, *e.g.*, via using a small τ ($\tau = 0.02$) to learn all discriminative signals into f_i^+ , does not yield more optimal performance, as shown in Fig. 6; and 2) the resulting f_i^* (calibrated from f_i^-) yields significant performance improvement, proving that f_i^- is rich with entangled class-relevant clues, as indicated in Table 7.

4.2. Domain Feature Corrector (DFC)

We then aim to calibrate the domain-related features f_i^- to capture additional discriminative clues that may complement f_i^+ , thereby promoting the local model to yield more consistent decisions for samples with the same class across domains. To this end, we design a Domain Feature Corrector (DFC) \mathcal{A}_C that takes the domain-related features f_i^- as input and produces their rectified features f_i^* . We implement the corrector \mathcal{A}_C as the same two-layer CNN architecture as the decoupler \mathcal{A}_D . In particular, \mathcal{A}_C learns the residual term [10] for more flexible training:

$$f_i^* = f_i^- + (1 - \mathcal{M}_i) \odot \mathcal{A}_C(f_i^-), \quad (6)$$

where \mathcal{M}_i is the pseudo-binary mask matrix in Eq. (3), and \odot represents an element-wise product operator.

The intended goal of our corrector is to enable rectified features f_i^* to provide useful clues that steer the local model toward more correct decisions. Therefore, we optimize the corrector \mathcal{A}_C by explicitly injecting correct discriminative semantic signals, which is formulated as:

$$\mathcal{L}_{DFC} = -y_i \cdot \log(\delta(\mathbf{m}(l_i^*))), \text{ s.t. } l_i^* = r_k^F(f_i^*), \quad (7)$$

where r_k^F consists of a pooling layer and a flattening operation to encode f_i^* as $l_i^* \in \mathbb{R}^d$, δ is a Softmax function, and \mathbf{m} is the same as the single-layer MLP in Eq. (5). By minimizing Eq. (7), we promote the corrector \mathcal{A}_C to regulate the domain-related features f_i^- to the rectified features f_i^* , thereby capturing additional class-relevant information. We then combine the domain-robust features f_i^+ and the rectified features f_i^* to obtain the final feature map $\tilde{f}_i = (f_i^+ + f_i^*) \in \mathbb{R}^{C \times H \times W}$, which is further passed to the subsequent layers of the local model.

Besides, the standard Cross-Entropy [34] loss is used on top of the logits ℓ_i with y_i to optimize the local model:

$$\mathcal{L}_{CE} = -\mathbf{1}_{y_i} \log(\delta(\ell_i)), \text{ s.t. } \ell_i = h(\theta_k; r_k^F(\tilde{f}_i)), \quad (8)$$

where δ represents a Softmax function, and $h(\theta_k; \cdot)$ is the classifier of the local model. Overall, we define the following objective for the local training of each client k as:

$$\mathcal{L} = \mathcal{L}_{CE} + \frac{1}{|L|} \sum_{j=1}^{|L|} (\lambda_1 \cdot \mathcal{L}_{DFD}^{L_j} + \lambda_2 \cdot \mathcal{L}_{DFC}^{L_j}), \quad (9)$$

where $\mathcal{L}_{DFD}^{L_j}$ and $\mathcal{L}_{DFC}^{L_j}$ mean the losses \mathcal{L}_{DFD} and \mathcal{L}_{DFC} calculated after the L_j backbone layer of the local model’s feature extractor, respectively. By default, we only calculate the losses \mathcal{L}_{DFD} and \mathcal{L}_{DFC} after the last backbone layer of the feature extractor ($|L| = 1$) for each client. λ_1 and λ_2 are hyper-parameters used to balance these loss terms.

4.3. Domain-Aware Aggregation

During the global aggregation phase, under domain-skewed FL scenario, the solution of naively performing average aggregation [31] is biased and neglects the domain diversity, resulting in restricted model performance. To mitigate this issue, we consider incorporating the domain discrepancy of each client into the global model’s aggregation process in a domain-aware manner. We first establish an ideal reference: a uniform global domain distribution, as it naturally promotes fairness across all domains for the same class. Then, we measure the distance between each local domain distribution and this uniform global domain distribution, treating it as a domain discrepancy.

Specifically, we define this uniform global domain distribution as a fixed vector $\mathcal{G} = [\frac{1}{Q}, \dots, \frac{1}{Q}] \in \mathbb{R}^C$, where Q denotes the number of domains and the value of each element in \mathcal{G} is $1/Q$ (e.g., for PACS [19], $Q = 4$). For client k , the

local domain distribution $\mathcal{B}_k = [\frac{n_k^1}{n^1}, \dots, \frac{n_k^C}{n^C}] \in \mathbb{R}^C$ is also abstracted as a vector, where $n_k^c \approx n_k/C$ and $n^c \approx N/C$ (under the domain skew, the label distribution is consistent). Therefore, we reformulate the local domain distribution of the client k as $\mathcal{B}_k = [\frac{n_k}{N}, \dots, \frac{n_k}{N}] \in \mathbb{R}^C$. Then, we calculate the domain discrepancy \mathbf{d}_k of the client k as follows:

$$\mathbf{d}_k = \sqrt{\frac{1}{2} \sum_{c=1}^C (\mathcal{B}_k^c - \mathcal{G}^c)^2}, \quad \mathcal{B}_k^c = \frac{n_k}{N}, \quad \mathcal{G}^c = \frac{1}{Q}, \quad (10)$$

where Q means the number of domains and $N = \sum_{k=1}^K n_k$. Based on Eq. (10), we obtain the domain discrepancy \mathbf{d}_k for each client k . We then enforce that the client k with a larger dataset size n_k and smaller domain discrepancy \mathbf{d}_k receives a higher aggregation weight \mathbf{p}_k :

$$\mathbf{p}_k = \frac{\epsilon(\alpha \cdot \frac{n_k}{N} - \beta \cdot \mathbf{d}_k)}{\sum_{j=1}^K \epsilon(\alpha \cdot \frac{n_j}{N} - \beta \cdot \mathbf{d}_j)}, \quad (11)$$

where ϵ denotes Sigmoid function, α and β are used to balance the n_k and \mathbf{d}_k . According to Eq. (11), even if the client dataset size is large (e.g., the dominant domain), we can determine a more distinguishing weight for each client rather than a simple average. Finally, we obtain the global model $w^* = \sum_{k=1}^K \mathbf{p}_k \cdot w_k$ in a domain-aware manner.

The global model is then broadcast to each participating client as the initialization for the next round’s local updating. Note that each client decoupler \mathcal{A}_D , corrector \mathcal{A}_C , and \mathbf{m} are kept locally, without participating in aggregation.

4.4. Summary and Discussion

In each communication round, the local model is trained on its private dataset by optimizing \mathcal{L} in Eq. (9), then the server collects these local weights to obtain the global model in a domain-aware aggregation manner, which is subsequently distributed to each participant as the initialization in the next communication round. The overview of $F^2\text{DC}$ is shown in Fig. 3, and a detailed algorithm is presented in Algorithm 1.

Besides, the modularity of our proposed $F^2\text{DC}$ suggests its broad scope of application. On the one hand, our decoupler \mathcal{A}_D and corrector \mathcal{A}_C can be easily incorporated with existing FL approaches to promote more robust local decisions. On the other hand, integrating the domain discrepancy into the global aggregation helps improve consensus among clients for the domain-skewed FL scenario. Empirically, enhancing FedAvg [31] with only our domain feature decoupler and corrector yields 8.94% performance gain on PACS [19], please refer to the details in Table 3.

5. Experiments

5.1. Experimental Setup

Datasets. We conduct our experiments on the following three popular multi-domain datasets:

Algorithm 1: Pseudo-code Flow of F^2 DC

Input: Communication Rounds R , Local Epochs E , Clients K , k -th client’s data \mathcal{D}_k and model w_k
Output: The final FL global model w_R^*

```
for each communication round  $r = 1, 2, \dots, R$  do
   $\mathcal{K}_r \leftarrow \{1, \dots, K\}$  // randomly select clients
  for each client  $k \in \mathcal{K}_r$  in parallel do
     $w_k \leftarrow \text{LocalUpdating}(w_r^*)$ 
  end
  /* Domain-Aware Aggregation (Sec.4.3) */
   $\mathbf{d}_k \leftarrow (\mathcal{B}_k, \mathcal{G})$  in Eq. (10) // discrepancy
   $\mathbf{p}_k \leftarrow (\mathbf{d}_k, n_k)$  in Eq. (11) // determine weight
   $w_{r+1}^* \leftarrow \sum_{k=1}^{|\mathcal{K}_r|} \mathbf{p}_k \cdot w_k$  // global model
end
LocalUpdating( $w_r^*$ ):
 $w_k \leftarrow w_r^* + \{\mathcal{A}_D, \mathcal{A}_C, \mathbf{m}\}$  // distribute
for each local epoch  $e = 1, 2, \dots, E$  do
  for each batch  $b \in$  private data  $\mathcal{D}_k$  do
    /* DFD Module (Sec.4.1) */
     $\mathcal{M}_i \leftarrow (\mathcal{A}_D, f_i)$  in Eq. (3) // mask matrix
     $f_i^+, f_i^- \leftarrow (\mathcal{M}_i, f_i)$  in Eq. (4) // decoupling
     $\mathcal{L}_{DFD}(f_i^+, f_i^-, y_i, \hat{y}_i, \mathbf{m})_{i \in b} \leftarrow$  Eq. (5)
    /* DFC Module (Sec.4.2) */
     $f_i^* \leftarrow (\mathcal{A}_C, \mathcal{M}_i, f_i^-)$  in Eq. (6) // calibrate
     $\mathcal{L}_{DFC}(f_i^*, y_i, \mathbf{m})_{i \in b} \leftarrow$  Eq. (7)
     $\mathcal{L}_{CE}(\ell_i, y_i)_{i \in b} \leftarrow$  Eq. (8)
     $\mathcal{L} = \mathcal{L}_{CE} + \frac{1}{|L|} \sum_{j=1}^{|L|} (\lambda_1 \cdot \mathcal{L}_{DFD}^{L_j} + \lambda_2 \cdot \mathcal{L}_{DFC}^{L_j})$ 
     $w_k \leftarrow w_k - \eta \nabla \mathcal{L}(w_k; b)$  // update model
  end
end
 $w_k \leftarrow w_k - \{\mathcal{A}_D, \mathcal{A}_C, \mathbf{m}\}$  // keep locally
return  $w_k$  to the server
```

- Digits [33] includes four domains as MNIST (M), USPS (U), SVHN (SV), and SYN (SY), with 10 categories.
- Office-Caltech [18] consists of four domains as Caltech (C), Amazon (A), Webcam (W), and DSLR (D), each is formed of 10 overlapping categories.
- PACS [19] consists of four domains as Photo (P), Art-Painting (AP), Cartoon (Ct), Sketch (Sk). Each domain contains 7 categories.

Domain-Skewed FL Scenarios. Following [5], we initialize 20, 10, and 10 clients for the Digits, Office-Caltech, and PACS, respectively. The allocation of domains to these clients is randomly generated and then fixed: Digits (M: 3, U: 6, SV: 6, SY: 5), Office-Caltech (C: 3, A: 2, W: 2, D: 3), PACS (P: 2, AP: 3, Ct: 2, Sk: 3). For each client, the local data is randomly selected from the allocated domains with 1% (Digits), 20% (Office-Caltech), and 30% (PACS).

Model Architecture. To facilitate a fair comparison, we use ResNet-10 [10] to conduct experiments, with the dimension $d = 512$. All compared methods use the same model.

Compared Methods. We compare F^2 DC with four types of state-of-the-art (SOTA) baselines: 1) standard FedAvg [31], FedProx [23]; 2) contrast-based MOON [20], FedRCL [36]; 3) prototype-based FPL [13], FedTGP [53], FedSA [57]; and 4) consensus-based FedHEAL [5], FDSE [48]. Among these methods, FPL [13], FedHEAL [5], and FDSE [48] are designed for the domain-skewed FL.

Implement Details. Unless otherwise mentioned, we run $R = 100$ global communication rounds, and the number of clients K is set to 20, 10, and 10 for Digits, Office-Caltech, and PACS datasets, respectively. All methods have little or no accuracy gain with more rounds R . We follow [20, 23] and use the SGD optimizer to update models with a learning rate η of 0.01, a momentum of 0.9, a batch size of 64, and a weight decay of 10^{-5} , with local epochs as $E = 10$. The dimension d of the embedding is 512. We empirically set the σ in Eq. (3) as 0.1, the τ in Eq. (5) as 0.06, $\lambda_1 = 0.8$ and $\lambda_2 = 1.0$ in Eq. (9), $\alpha = 1.0$ and $\beta = 0.4$ in Eq. (11). We implement the decoupler \mathcal{A}_D in Sec. 4.1 and corrector \mathcal{A}_C in Sec. 4.2 as a two-layer CNN architecture with batch normalization and ReLU activation, the input and output are both $\in \mathbb{R}^{C \times H \times W}$. The \mathbf{m} in Eq. (5) and Eq. (7) is a single-layer MLP architecture to predict the logits as $\mathbb{R}^d \rightarrow \mathbb{R}^C$. By default, we insert \mathcal{A}_D and \mathcal{A}_C after the last backbone layer of the feature extractor of the local model.

Evaluation Metrics. Following [23, 24], we use top-1 accuracy in each domain, and average (AVG) and standard deviation (STD) of accuracy across domains as evaluation metrics. All results reported are the average of three independent runs with different random seeds.

5.2. Main Results

Comparison to SOTA Methods. Table 1 and Table 2 provide the comparison results of our F^2 DC and nine competing methods on Digits, Office-Caltech, and PACS. These results empirically indicate that F^2 DC consistently outperforms other methods, which confirms that our method acquires well-generalizable ability across different domains and promotes cross-domain fairness (*i.e.*, with a smaller STD). Additionally, we observe that contrast-based methods (*e.g.*, MOON, FedRCL) perform poorly, even significantly worse than FedAvg on PACS. This may be because forcing the local models to align with compromised global representations through a contrastive scheme is detrimental and further exacerbates the performance degradation. This underscores the importance of promoting local training away from client-specific domain biases. Unlike the elimination-based, domain-skewed FL method FDSE, F^2 DC liberates additional class-relevant clues by calibrating domain-specific biased features, enabling more correct decisions across different domains.

Table 1. **Comparison results** on Office-Caltech and PACS. Best results are in **red bold**, with second best in **blue bold**.

Methods	Office-Caltech						PACS					
	Caltech	Amazon	Webcam	DSLR	AVG \uparrow	STD \downarrow	Photo	Art-Paint	Cartoon	Sketch	AVG \uparrow	STD \downarrow
FedAvg [AISTATS'17]	59.82	65.26	51.72	46.67	55.86	8.27	60.98	52.49	74.63	77.46	66.39	11.74
FedProx [MLSys'20]	60.18	66.11	54.96	47.30	57.13	7.98	61.88	57.40	76.34	80.14	68.94	11.00
MOON [CVPR'21]	57.14	63.16	44.48	40.87	51.41	10.49	59.72	50.29	70.35	70.22	62.64	9.63
FPL [CVPR'23]	60.05	65.53	52.90	64.45	60.73	5.75	66.67	58.38	79.75	77.59	70.59	9.95
FedTGP [AAAI'24]	61.28	63.84	53.37	63.68	60.54	4.92	60.68	56.06	75.27	78.03	67.51	10.78
FedRCL [CVPR'24]	60.27	65.89	48.72	50.14	56.24	8.64	61.37	55.17	70.78	76.57	65.97	9.54
FedHEAL [CVPR'24]	61.02	67.47	55.36	62.99	61.71	4.95	70.39	65.82	80.57	76.61	73.34	6.54
FedSA [AAAI'25]	63.52	66.21	56.90	58.93	61.39	4.24	68.55	60.42	78.32	75.50	70.69	7.98
FDSE [CVPR'25]	60.39	66.80	58.31	67.20	63.18	4.50	69.27	65.46	78.65	79.12	73.13	6.83
F^2DC (Ours)	62.95	68.42	64.79	71.12	66.82	3.65	75.15	68.71	79.91	82.11	76.47	5.83

Table 2. **Comparison results** on Digits, continuing Table 1.

Methods	Digits					
	MNIST	USPS	SVHN	SYN	AVG \uparrow	STD \downarrow
FedAvg	96.04	89.84	88.04	51.05	81.24	20.42
FedProx	96.13	89.04	87.56	51.00	80.93	20.30
MOON	94.70	89.64	87.68	34.40	76.60	28.29
FPL	96.12	89.94	89.15	49.15	81.09	21.52
FedTGP	95.38	87.49	87.37	49.40	79.91	20.68
FedRCL	93.08	89.73	84.98	51.20	79.75	19.32
FedHEAL	96.39	87.00	89.41	56.95	82.43	17.45
FedSA	94.85	90.74	88.48	57.41	82.87	17.18
FDSE	95.17	90.34	90.98	60.13	84.15	16.19
F^2DC (Ours)	97.75	92.94	90.53	67.69	87.23	13.36

Table 3. **Modularity** of F^2 DC on PACS, where we plug-in our proposed DFD and DFC into four strong baselines.

Methods	P	AP	Ct	Sk	AVG \uparrow					
FedAvg	74.86	\uparrow 13.88	65.90	\uparrow 13.41	79.70	\uparrow 5.07	80.86	\uparrow 3.40	75.33	\uparrow 8.94
FPL	76.85	\uparrow 10.18	64.46	\uparrow 6.08	80.02	\uparrow 0.27	80.75	\uparrow 3.16	75.52	\uparrow 4.93
FedHEAL	75.56	\uparrow 5.17	65.95	\uparrow 0.13	81.27	\uparrow 0.70	77.48	\uparrow 0.87	75.06	\uparrow 1.72
FDSE	72.25	\uparrow 2.98	65.99	\uparrow 0.53	80.56	\uparrow 1.91	80.36	\uparrow 1.24	74.79	\uparrow 1.66

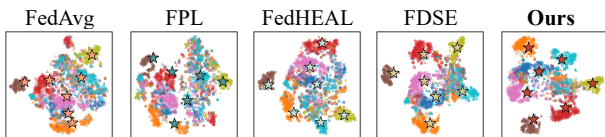


Figure 4. **T-SNE visualization** on PACS. Each color means one class, each shape means one domain, stars are semantic centers.

Improving Performance of Existing FL Methods. One key advantage of F^2 DC is its modularity. As shown in Table 3, we report the results of baselines combined with our DFD and DFC modules, detailing both the resulting accuracy and the performance gain over the original methods. The results indicate that our two modules consistently enhance performance in multiple domains. FedAvg yields the largest benefit and achieves 8.94% average accuracy gain over its original version.

Table 4. **Efficiency comparison** per round (10 clients) on PACS.

Methods	Upload $\times 10^7$	Comm.	FLOPs $\times 10^{10}$	Time _{train}
FedAvg	5.43	193.72MB	16.31	176.94s
FPL	5.45	197.30MB	19.45	215.61s
FedHEAL	5.43	193.72MB	16.70	186.92s
F^2DC	5.43	193.72MB	16.46	180.67s

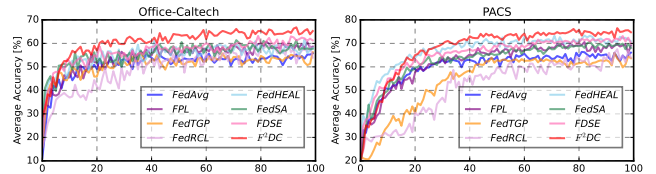


Figure 5. **Comparison of convergence in average accuracy** on Office-Caltech (Left) and PACS (Right). Zoom in for details.

T-SNE Visualization. Fig. 4 depicts the t-SNE [40] visualization of the representation space for different FL methods on PACS. Compared to these four strong baselines, 1) F^2 DC enhances the inter-class separability, *i.e.*, greater distance between samples of different colors compared to other methods; and 2) F^2 DC reduces the intra-class distance among samples of the same color, resulting in tighter clustering. This further indicates F^2 DC’s ability to establish consistent semantic representations and decision boundaries across diverse domains.

Efficiency Analysis. Table 4 provides the communication and computation cost on the PACS dataset with 10 clients. Compared to FedAvg, F^2 DC incurs no additional communication cost. F^2 DC attains superior performance with a modest computational cost, where the additional training cost mainly stems from the decoupler and corrector.

Convergence. In Fig. 5, we plot the average accuracy per round for various FL methods. It can be observed that our F^2 DC exhibits a faster convergence speed, and ultimately achieves higher performance as training progresses.

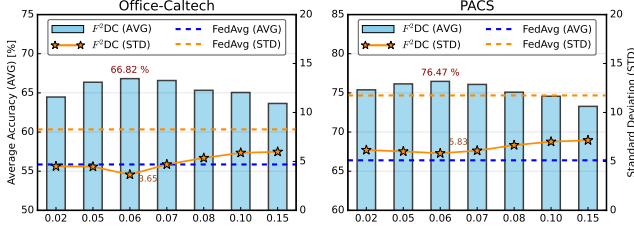


Figure 6. Hyper-parameter study with different τ of Eq. (5).

Table 5. Hyper-parameter study with σ of Eq. (3) on PACS.

σ	0.01	0.05	0.1	0.3	0.5	1.0	5.0
AVG \uparrow	74.81	75.19	76.47	75.34	74.40	74.15	73.86
STD \downarrow	6.48	6.32	5.83	6.35	6.71	7.05	7.23



Figure 7. Hyper-parameter study with α and β of Eq. (11).

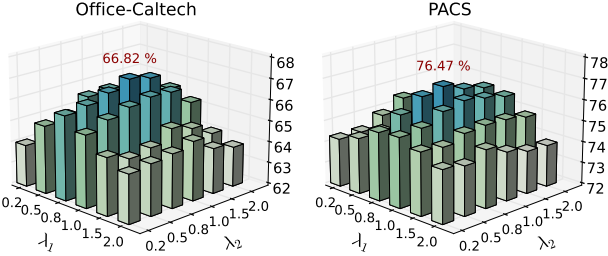


Figure 8. Hyper-parameter study with λ_1 and λ_2 of Eq. (9).

5.3. Validation Analysis

Hyper-parameter Study. We first examine the impact of hyper-parameter τ (Eq. (5)) in Fig. 6, which reveals that a smaller τ benefits feature separation more than higher ones. We observe that F^2DC is not sensitive to $\tau \in [0.05, 0.07]$ and the optimal performance is reached when $\tau = 0.06$.

We then report the effect of hyper-parameter σ (Eq. (3)) that controls the discreteness of the mask matrix in Table 5. For the low σ values, mask matrix \mathcal{M}_i of Eq. (3) becomes more discrete; for high values, \mathcal{M}_i becomes more uniform. The value of σ that is too small (\rightarrow binary sampling) or too large (\rightarrow uniform sampling) hinders training.

We investigate α and β of Eq. (11) for a wide range, and show the accuracy in Fig. 7. We observe that F^2DC brings performance improvement by incorporating domain discrepancy. Generally, $\alpha \in [0.8, 1.2]$ and $\beta \in [0.3, 0.5]$ is a suitable choice for domain-aware aggregation, leading to stable and competitive performance in F^2DC . Besides, we present the accuracy for diverse λ_1 and λ_2 of Eq. (9)

Table 6. Ablation study of key modules in our F^2DC on Office-Caltech (Top) and PACS (Bottom). Please see details in Sec. 5.3.

\mathcal{L}_{DFD}	\mathcal{L}_{DFC}	DaA	C	A	W	D	AVG \uparrow	STD \downarrow
			59.82	65.26	51.72	46.67	55.86	8.27
		✓	60.25	65.79	54.39	50.33	57.69	6.76
✓		✓	66.68	67.53	56.55	60.02	62.70	5.30
✓	✓		63.71	68.21	59.07	67.62	64.65	4.22
✓	✓	✓	60.84	67.79	62.10	70.45	65.29	4.57
✓	✓	✓	62.95	68.42	64.79	71.12	66.82	3.65
\mathcal{L}_{DFD}	\mathcal{L}_{DFC}	DaA	P	AP	Ct	Sk	AVG \uparrow	STD \downarrow
			60.98	52.49	74.63	77.46	66.39	11.74
		✓	61.28	57.64	75.71	79.09	68.43	10.15
✓		✓	72.95	61.52	79.06	80.13	73.41	8.35
✓	✓		72.55	65.44	77.61	78.95	73.64	6.12
✓	✓	✓	74.86	65.90	79.70	80.86	75.33	6.80
✓	✓	✓	75.15	68.71	79.91	82.11	76.47	5.83

Table 7. Ablation study of F^2DC 's various features on PACS.

Protocols	P	AP	Ct	Sk	AVG \uparrow	STD \downarrow
f^+	74.21	67.52	78.35	80.47	75.13	5.90
f^-	59.45	50.09	52.56	69.37	57.87	8.63
f^*	74.83	64.05	75.80	79.29	73.49	6.71
\tilde{f}	75.15	68.71	79.91	82.11	76.47	5.83

in Fig. 8. The results show that F^2DC maintains consistent performance across varying λ_1 and λ_2 values, but extremely large λ_1 or λ_2 lead to optimization instability. The accuracy amelioration becomes marginal when $\alpha = 1.0, \beta = 0.4$ in Fig. 7 and $\lambda_1 = 0.8, \lambda_2 = 1.0$ in Fig. 8.

Ablation Study. We conduct an ablation study in Table 6 (first row refers to FedAvg [31]). We observe that each component contributes positively to the overall performance, and their combination yields the optimal performance. This supports our motivation to decouple local features via DFD and then calibrate the domain-biased features via DFC.

In Table 7, we then report the results of using various features obtained by F^2DC on PACS. Results show that f^+ is significantly better than f^- , indicating our decoupler effectively disentangles local features. Compared to f^- , f^* yields consistent improvements, suggesting that f^* captures additional class-relevant clues for cross-domain decisions.

6. Conclusion

In this paper, we propose Federated Feature Decoupling and Calibration (F^2DC) for domain-skewed FL. To achieve this, F^2DC disentangles local features and corrects domain-biased features to capture additional useful clues, while performing domain-aware aggregation to promote consensus among clients. Extensive experimental results demonstrate the effectiveness and modularity of our proposed F^2DC .

Acknowledgment

This work is partially supported by the Australian Research Council Linkage Project LP210300009 and LP230100083, the Singapore Ministry of Education (MOE) Academic Research Fund (AcRF) Tier 1 Grant (24-SIS-SMU-008), A*STAR under its MTC YIRG Grant (M24N8c0103), and the Lee Kong Chian Fellowship (T050273).

References

- [1] Sikai Bai, Jie Zhang, Song Guo, Shuaicheng Li, Jingcai Guo, Jun Hou, Tao Han, and Xiaocheng Lu. Diprompt: Disentangled prompt tuning for multiple latent domain generalization in federated learning. In *CVPR*, pages 27284–27293, 2024. 3
- [2] Cosmin I Bercea, Benedikt Wiestler, Daniel Rueckert, and Shadi Albarqouni. Federated disentangled representation learning for unsupervised brain anomaly detection. *Nature Machine Intelligence*, 4(8):685–695, 2022. 3
- [3] Zhaowei Cai and Nuno Vasconcelos. Rethinking differentiable search for mixed-precision neural networks. In *CVPR*, pages 2349–2358, 2020. 4
- [4] Jiayi Chen and Aidong Zhang. On disentanglement of asymmetrical knowledge transfer for modality-task agnostic federated learning. In *AAAI*, pages 11311–11319, 2024. 3
- [5] Yuhang Chen, Wenke Huang, and Mang Ye. Fair federated learning under domain skew with local consistency and domain diversity. In *CVPR*, pages 12077–12086, 2024. 3, 6
- [6] Lele Fu, Sheng Huang, Yanyi Lai, Tianchi Liao, Chuanfu Zhang, and Chuan Chen. Beyond federated prototype learning: Learnable semantic anchors with hyperspherical contrast for domain-skewed data. In *AAAI*, pages 16648–16656, 2025. 3
- [7] Lele Fu, Sheng Huang, Yanyi Lai, Chuanfu Zhang, Hong-Ning Dai, Zibin Zheng, and Chuan Chen. Federated domain-independent prototype learning with alignments of representation and parameter spaces for feature shift. *IEEE Transactions on Mobile Computing*, 24(9):9004–9019, 2025. 2
- [8] Marco Fumero, Florian Wenzel, Luca Zancato, Alessandro Achille, Emanuele Rodolà, Stefano Soatto, Bernhard Schölkopf, and Francesco Locatello. Leveraging sparse and shared feature activations for disentangled representation learning. In *NeurIPS*, pages 27682–27698, 2023. 3
- [9] Liang Gao, Huazhu Fu, Li Li, Yingwen Chen, Ming Xu, and Cheng-Zhong Xu. Feddc: Federated learning with non-iid data via local drift decoupling and correction. In *CVPR*, pages 10112–10121, 2022. 3
- [10] Kaiming He, Xiangyu Zhang, Shaoqing Ren, and Jian Sun. Deep residual learning for image recognition. In *CVPR*, pages 770–778, 2016. 3, 4, 6
- [11] Sheng Huang, Lele Fu, Tianchi Liao, Bowen Deng, Chuanfu Zhang, and Chuan Chen. Fedbg: Proactively mitigating bias in cross-domain graph federated learning using background data. In *IJCAI*, pages 5408–5416, 2025. 3
- [12] Wenke Huang, Mang Ye, and Bo Du. Learn from others and be yourself in heterogeneous federated learning. In *CVPR*, pages 10143–10153, 2022. 3
- [13] Wenke Huang, Mang Ye, Zekun Shi, He Li, and Bo Du. Rethinking federated learning with domain shift: A prototype view. In *CVPR*, pages 16312–16322, 2023. 3, 6
- [14] Wenke Huang, Mang Ye, Zekun Shi, Guancheng Wan, He Li, Bo Du, and Qiang Yang. Federated learning for generalization, robustness, fairness: A survey and benchmark. *IEEE TPAMI*, 46(12):9387–9406, 2024. 3
- [15] Meirui Jiang, Zirui Wang, and Qi Dou. Harmoff: Harmonizing local and global drifts in federated learning on heterogeneous medical images. In *AAAI*, pages 1087–1095, 2022. 3
- [16] Peter Kairouz, H Brendan McMahan, Brendan Avent, Aurélien Bellet, et al. Advances and open problems in federated learning. *Foundations and Trends in Machine Learning*, 14(1):1–210, 2021. 1
- [17] Sai Praneeth Karimireddy, Satyen Kale, Mehryar Mohri, Sashank Reddi, Sebastian Stich, and Ananda Theertha Suresh. Scaffold: Stochastic controlled averaging for federated learning. In *ICML*, pages 5132–5143, 2020. 1
- [18] Boqing Kong, Yuan Shi, Fei Sha, and Kristen Grauman. Geodesic flow kernel for unsupervised domain adaptation. In *CVPR*, pages 2066–2073, 2012. 6
- [19] Da Li, Yongxin Yang, Yi-Zhe Song, and Timothy M Hospedales. Deeper, broader and artier domain generalization. In *ICCV*, pages 5542–5550, 2017. 1, 3, 5, 6
- [20] Qinbin Li, Bingsheng He, and Dawn Song. Model-contrastive federated learning. In *CVPR*, pages 10713–10722, 2021. 6
- [21] Qinbin Li, Yiqun Diao, Quan Chen, and Bingsheng He. Federated learning on non-iid data silos: An experimental study. In *ICDE*, pages 965–978, 2022. 1, 3
- [22] Tian Li, Anit Kumar Sahu, Ameet Talwalkar, and Virginia Smith. Federated learning: Challenges, methods, and future directions. *IEEE Signal Processing Magazine*, 37(3):50–60, 2020. 1
- [23] Tian Li, Anit Kumar Sahu, Manzil Zaheer, Maziar Sanjabi, Ameet Talwalkar, and Virginia Smith. Federated optimization in heterogeneous networks. In *MLSys*, pages 429–450, 2020. 1, 3, 6
- [24] Tian Li, Maziar Sanjabi, Ahmad Beirami, and Virginia Smith. Fair resource allocation in federated learning. In *ICLR*, 2020. 6
- [25] Xiang Li, Kaixuan Huang, Wenhao Yang, Shusen Wang, and Zhihua Zhang. On the convergence of fedavg on non-iid data. In *ICLR*, 2020. 1, 3
- [26] Xiang Li, Yasushi Makihara, Chi Xu, Yasushi Yagi, and Mingwu Ren. Gait recognition via semi-supervised disentangled representation learning to identity and covariate features. In *CVPR*, pages 13309–13319, 2020. 3
- [27] Yichen Li, Wenchao Xu, Haozhao Wang, Yining Qi, Jingcai Guo, and Ruixuan Li. Personalized federated domain-incremental learning based on adaptive knowledge matching. In *ECCV*, pages 127–144, 2024. 3
- [28] Zhiwei Li, Guodong Long, Tianyi Zhou, Jing Jiang, and Chengqi Zhang. Personalized federated collaborative filtering: A variational autoencoder approach. In *AAAI*, pages 18602–18610, 2025. 3

- [29] Christos Louizos, Max Welling, and Diederik P Kingma. Learning sparse neural networks through l_0 regularization. In *ICLR*, 2018. 4
- [30] Jianxin Ma, Chang Zhou, Peng Cui, Hongxia Yang, and Wenwu Zhu. Learning disentangled representations for recommendation. In *NeurIPS*, pages 5711–5722, 2019. 3
- [31] Brendan McMahan, Eider Moore, Daniel Ramage, Seth Hampson, and Blaise Aguerre y Arcas. Communication-efficient learning of deep networks from decentralized data. In *AISTATS*, pages 1273–1282, 2017. 1, 2, 3, 5, 6, 8
- [32] Yujie Mo, Yajie Lei, Jialie Shen, Xiaoshuang Shi, Heng Tao Shen, and Xiaofeng Zhu. Disentangled multiplex graph representation learning. In *ICML*, pages 24983–25005, 2023. 3
- [33] Xingchao Peng, Qinxun Bai, Xide Xia, Zijun Huang, Kate Saenko, and Bo Wang. Moment matching for multi-source domain adaptation. In *ICCV*, pages 1406–1415, 2019. 6
- [34] De Boer Pieter-Tjerk, Dirk P Kroese, Shie Mannor, and Reuven Rubinfeld. A tutorial on the cross-entropy method. *Annals of Operations Research*, 134(1):19–67, 2005. 5
- [35] Ramprasaath R Selvaraju, Michael Cogswell, Abhishek Das, Ramakrishna Vedantam, Devi Parikh, and Dhruv Batra. Grad-cam: Visual explanations from deep networks via gradient-based localization. In *ICCV*, pages 618–626, 2017. 2
- [36] Seonguk Seo, Jinkyu Kim, Geeho Kim, and Bohyung Han. Relaxed contrastive learning for federated learning. In *CVPR*, pages 12279–12288, 2024. 6
- [37] Benyuan Sun, Hongxing Huo, Yi Yang, and Bo Bai. Partialfed: Cross-domain personalized federated learning via partial initialization. In *NeurIPS*, pages 23309–23320, 2021. 3
- [38] Canh T Dinh, Nguyen Tran, and Josh Nguyen. Personalized federated learning with moreau envelopes. In *NeurIPS*, pages 21394–21405, 2020. 3
- [39] Md Palash Uddin, Yong Xiang, Xuequan Lu, John Yearwood, and Longxiang Gao. Federated learning via disentangled information bottleneck. *IEEE Transactions on Services Computing*, 16(3):1874–1889, 2022. 3
- [40] Laurens van der Maaten and Geoffrey Hinton. Visualizing data using t-sne. *Journal of Machine Learning Research*, 9(86):2579–2605, 2008. 7
- [41] Feng Wang and Huaping Liu. Understanding the behaviour of contrastive loss. In *CVPR*, pages 2495–2504, 2021. 4
- [42] Haozhao Wang, Haoran Xu, Yichen Li, Yuan Xu, et al. Fedcda: Federated learning with cross-rounds divergence-aware aggregation. In *ICLR*, 2024. 1, 3
- [43] Huan Wang, Haoran Li, Huaming Chen, Jun Yan, Jiahua Shi, and Jun Shen. Feddifrc: Unlocking the potential of text-to-image diffusion models in heterogeneous federated learning. In *ICCV*, pages 3726–3736, 2025. 1
- [44] Huan Wang, Haoran Li, Huaming Chen, Jun Yan, Jiahua Shi, and Jun Shen. Fedsc: Federated learning with semantic-aware collaboration. In *ACM SIGKDD*, pages 2938–2949, 2025. 3
- [45] Huan Wang, Haoran Li, Huaming Chen, Jun Yan, Lijuan Wang, Jiahua Shi, Shiping Chen, and Jun Shen. Fedskc: Federated learning with non-iid data via structural knowledge collaboration. In *IEEE International Conference on Web Services*, pages 702–712, 2025. 3
- [46] Xin Wang, Hong Chen, Si’ao Tang, Zihao Wu, and Wenwu Zhu. Disentangled representation learning. *IEEE TPAMI*, 46(12):9677–9696, 2024. 3
- [47] Yuan Wang, Huazhu Fu, Renuga Kanagavelu, Qingsong Wei, et al. An aggregation-free federated learning for tackling data heterogeneity. In *CVPR*, pages 26233–26242, 2024. 1, 3
- [48] Zheng Wang, Zihui Wang, Xiaoliang Fan, and Cheng Wang. Federated learning with domain shift eraser. In *CVPR*, pages 4978–4987, 2025. 2, 3, 6
- [49] Haoran Xu, Jiaze Li, Wanyi Wu, and Hao Ren. Federated learning with sample-level client drift mitigation. In *AAAI*, pages 21752–21760, 2025. 3
- [50] Peng Yan and Guodong Long. Personalization disentanglement for federated learning. In *ICME*, pages 318–323, 2023. 3
- [51] Rui Ye, Mingkai Xu, Jianyu Wang, Chenxin Xu, Siheng Chen, and Yanfeng Wang. Feddisco: Federated learning with discrepancy-aware collaboration. In *ICML*, pages 39879–39902, 2023. 1, 3
- [52] Jianqing Zhang, Yang Hua, Hao Wang, Tao Song, Zhengui Xue, Ruhui Ma, and Haibing Guan. Fedala: Adaptive local aggregation for personalized federated learning. In *AAAI*, pages 11237–11244, 2023. 3
- [53] Jianqing Zhang, Yang Liu, Yang Hua, and Jian Cao. Fedtgp: Trainable global prototypes with adaptive-margin-enhanced contrastive learning for data and model heterogeneity in federated learning. In *AAAI*, pages 16768–16776, 2024. 6
- [54] Jianqiao Zhang, Caifeng Shan, and Jungong Han. Fedgmkd: An efficient prototype federated learning framework through knowledge distillation and discrepancy-aware aggregation. In *NeurIPS*, pages 118326–118356, 2024. 3
- [55] Kaike Zhang, Qi Cao, Gaolin Fang, Bingbing Xu, Hongjian Zou, Huawei Shen, and Xueqi Cheng. Dyted: Disentangled representation learning for discrete-time dynamic graph. In *ACM SIGKDD*, pages 3309–3320, 2023. 3
- [56] Ziyuan Zhang, Luan Tran, Xi Yin, Yousef Atoum, Xiaoming Liu, Jian Wan, and Nanxin Wang. Gait recognition via disentangled representation learning. In *CVPR*, pages 4710–4719, 2019. 3
- [57] Yanbing Zhou, Xiangmou Qu, Chenlong You, Jiyang Zhou, Jingyue Tang, Xin Zheng, Chunmao Cai, and Yingbo Wu. Fedsa: A unified representation learning via semantic anchors for prototype-based federated learning. In *AAAI*, pages 23009–23017, 2025. 3, 6
- [58] Hangyu Zhu, Jinjin Xu, Shiqing Liu, and Yaochu Jin. Federated learning on non-iid data: A survey. *Elsevier Neurocomputing*, 465:371–390, 2021. 1, 3